Enhanced Photovoltaic Performance of Nanostructured Hybrid Solar Cell Using Highly Oriented TiO_2 Nanotubes

Supan Yodyingyong,[†,‡] Xiaoyuan Zhou,[†] Qifeng Zhang,[†] Darapond Triampo,[§] Junting Xi,[†] Kwangsuk Park,[†] Benjie Limketkai,[||] and Guozhong Cao*[,†]

Department of Materials Science and Engineering, University of Washington, Seattle, Washington 98195, United States, Institute for Innovative Learning, Mahidol University, 999 Phuttamonthon 4 Road, Nakhon Pathom 73170, Thailand, Department of Chemistry, Center of Excellence for Innovation in Chemistry, Faculty of Science, Mahidol University, Bangkok 10400, Thailand, and Intel Research Laboratories Seattle, Seattle, Washington 98105, United States

Received: August 17, 2010; Revised Manuscript Received: September 21, 2010

Highly oriented TiO_2 nanotubes have been fabricated using ZnO nanorod template through liquid reactive deposition on the ITO substrates. The diameter and length of TiO_2 nanotubes can be effectively controlled for the suitable use for a hybrid solar cell by varying the diameter and length of the ZnO nanorod template. A mixture of P3HT/PCBM was infiltrated into the gaps between TiO_2 nanotubes to form hybrid solar cells. The open circuit voltage, short circuit current density, fill factor, and power conversion efficiency of the hybrid solar cell using highly oriented TiO_2 nanotubes were 646 mV, 9.95 mA cm^{-2}, 51.6%, and 3.32%, respectively, much higher than 1.2% of hybrid solar cell based on ZnO nanorods tested under otherwise identical conditions and significantly higher than 0.7% of the same type hybrid solar cells reported in literature. The enhancement of the power conversion efficiency could be resulted from the highly oriented TiO_2 nanotubes with smaller diameter and large specific surface area for the efficient electron transfer in hybrid solar cells.

Introduction

The widespread use of inorganic solar cells remains limited due to the high costs of fabrication.[1] A lot of effort is being made to develop so-called third generation of solar cells including dye-sensitized solar cells, DSCs[2,3] and organic photovoltaics, OPVs.[4−6] OPVs or polymer-based photovoltaic devices can be processed from solution and have become a promising low cost alternative to traditional inorganic solar cell.[7−10] The key of the polymer solar cells is the bulk heterojunction, which is a blend of electron-donating semiconducting polymers and electron-withdrawing fullerides. This bulk heterojunction morphology enhances the interfacial area, where the photogenerated excitons, electron−hole pairs, are dissociated into charge carriers, and enables holes and electrons to be transported and collected. The power conversion efficiency (PCE) of the bulk heterojunction polymer solar cells which certified by the National Renewable Energy Laboratory (NREL) of up to 8.13% have been recently reported by Solarmer Energy, Inc.[11] However, polymer-based solar cells still suffer from low efficiencies and the limited lifetime as compared to silicon-based solar cell.[1] The limited efficiency of the bulk heterojunction polymer solar cell is due to the lower charge mobility in polymer,[12] the short exciton diffusion length, which can only diffuse around 20 nm,[13] the charge trapping in the conducting pathways of fullerides and polymer to the electrodes,[14] and the mismatch of the absorption spectrum of the active layer and the solar emission.[15,16] To address the intrinsic limitations of polymer solar cells, new strategies have been investigated such as the development of new polymers with a low bandgap for better match absorption of the solar spectrum,[17] and a hybrid organic/inorganic solar cells (hybrid solar cells), which are composed of an organic donor material and an *n*-type inorganic semiconductor.[18−23] These hybrid solar cells have the potential to combine the properties of physical stability and high charge mobility of inorganic materials and the potential of easy control of the active layer structure and interface morphology.

The hybrid solar cells using a vertically oriented TiO_2 nanotube or nanorod arrays filled with the blend of P3HT and PCBM have been investigated,[23−28] which have the advantages of both the bulk heterojunction and ordered architectures. The bulk heterojunction morphology provides the sufficient interfacial area for the separation of photogenerated excitons. The ordered architectures help to reduce the electron recombination and function as the direct pathway for fast electron transport to the charge collecting electrode. In addition, when a blend of P3HT and PCBM deposited on the vertically aligned TiO_2 nanotubes or nanorods, a double heterojunction structure is formed.[23,28,29] This help improved the power conversion efficiency by providing electron pathways from both TiO_2/PCBM interface and TiO_2/P3HT interface.

Oriented or ordered TiO_2 nanotubes can be readily prepared by anodizing titanium foils in an acidic electrolyte. Although anodization of Ti film has several advantages and the hybrid solar cells achieved a high power conversion efficiency of 4.7%,[28] a dense array, precise control of the nanotube configuration and a high throughput process cannot be guaranteed, and TiO_2 nanotube, fabricated by anodization of titanium foils, is difficult to use in the micro- and nanodevice applications.[30] More recently, Rattanavoravipa et al.[31] reported a one-step templating method to prepare highly aligned TiO_2 nanowire arrays (100−150 nm in diameter and 1 μm long), which uses ZnO nanorod obtained from aqueous solution route as a

* To whom correspondence should be addressed. E-mail: gzcao@u.washington.edu.
[†] University of Washington.
[‡] Institute for Innovative Learning, Mahidol University.
[§] Department of Chemistry, Mahidol University.
[||] Intel Research Laboratories Seattle.

10.1021/jp1077888
Published on Web 11/17/2010

template. However, for the application of hybrid solar cell, these TiO_2 nanostructures are either too densely populated, which would prevent the effective infiltration of polymer solution, or their diameters are too large, which limit the specific surface area, leading to less efficient charge separation, and a power conversion efficiency of 0.7% has been achieved.[31]

In this work, a simple fabrication method was employed for the growth of highly oriented TiO_2 nanotubes on indium-doped tin oxide (ITO) substrates by using ZnO nanorods as templates, which were formed by an aqueous solution route. The diameter and the length of TiO_2 nanotubes were carefully controlled for being used in the hybrid solar cell by varying the diameter and length of ZnO nanorod template. It was found that the hybrid solar cell based on these TiO_2 nanotubes infiltrated with P3HT and PCBM showed an enhanced power conversion efficiency of 3.32%, as compared to 0.7% reported in literature.[31]

Experimental Details

Synthesis of TiO_2 Nanotubes. The deposition was conducted via a three-step procedure. (1) Seed layers were first grown to block the injection of holes into ITO electrode. ITO substrates were cleaned by acetone/ethanol sonication. These freshly cleaned ITO glasses were used to deposit a thin layer of TiO_2 of thickness ~30 nm by immersing the substrate in a solution containing 0.1 M $(NH_4)_2TiF_6$ and 0.2 M H_3BO_3 for 30 min at 25 °C. The substrates were then spin coated by 0.60 mol L^{-1} of $Zn(CH_3COO)_2 \cdot 2H_2O$ in a 2-methoxyethanol/monoethanolamine to form ~50 nm thick seed layer of ZnO, followed by heat treatment at 300 °C for 10 min to obtain dense and transparent seed layers. (2) ZnO template growing. The seeded substrates were placed in an aqueous solution containing 0.015 M $Zn(NO_3)_2$ and 0.015 M hexamethylenetetramine at 95 °C for 2 h. Subsequently, the resultant films were thoroughly rinsed with deionized water (DI) to remove any residual salt or amino complex and dried with compressed air. (3) TiO_2 nanotube forming. The synthesized ZnO nanorod arrays on ITO were immersed in aqueous solution consisting of 0.075 M $(NH_4)_2TiF_6$ and 0.2 M H_3BO_3 at room temperature for 1.5 h. The resulting TiO_2 nanotubes were then dipped in a 0.5 M H_3BO_3 solution for 1 h to remove any residual ZnO. The products were then rinsed with DI water and calcined in air at 400 °C for 1 h. Crystallographic characterizations of the samples were performed in a Bruker D8 Focus X-ray diffractometer. The surface morphology and the fracture cross section of the specimens were obtained by scanning electron microscope (SEM, Philips, JEOL JSM7000) with an energy-dispersion X-ray analyzer.

Device Fabrication and Characterization. The chlorodebenzene solution containing 20 mg mL^{-1} P3HT (Reike Metal, Sepiolid P100) and 16 mg mL^{-1} PCBM (American Dye Source Inc. ADS61BFB) was stirred inside the glovebox for overnight at 60 °C and then spin coated at 1000 rpm onto the TiO_2 nanotube covered substrates, which were first air plasma treated for 15 min. The samples were then placed on a hot plate at 150 °C for 15 min to help self-organization of P3HT,[32] driving away residual water and assisting the polymer infiltration into the TiO_2 nanotube arrays.[28] A hole-transport layer of poly(3,4-ethylenedioxylene thiophene)−poly(styrene sulfonic acid) (PEDOT−PSS, Clevios P VP Al 4083) was subsequently spin-coated with a thickness of ~50 nm outside of the glovebox and filtered through a 0.45 μm filter. The films were baked at 120 °C for 10 min and then the devices were transferred into a deposition chamber inside the glovebox to deposit a 100 nm of Ag, which thermally evaporated under a vacuum of 2×10^{-6} Torr. The $J-V$ characteristics of solar cell were tested in air using a Keithley 2400 source measurement unit, and an Oriel Xenon lamp (450 W) coupled with an AM1.5 filter. A calibrated silicon reference solar cell certificated by the NREL was used to confirm the measurement conditions. A light intensity of 100 mW cm^{-2} was used in all the measurements in this study.

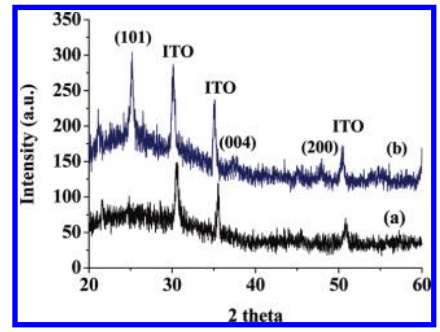

Figure 1. XRD patterns of the TiO_2 nanotube films before (a) and after (b) annealed at 400 °C.

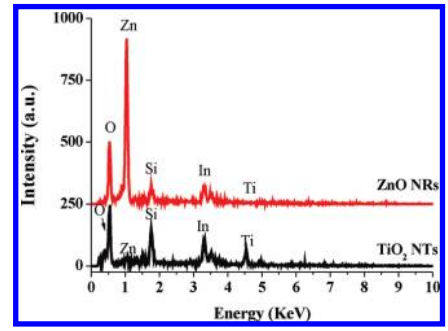

Figure 2. EDX spectra of ZnO nanorod (ZnO NRs) arrays and TiO_2 nanotube (TiO_2 NTs) arrays.

Results and Discussion

Figure 1 shows and compares the XRD patterns of the TiO_2 nanotube film before (Figure 1a) and after (Figure 1b) being annealed at 400 °C for 1 h in air. Before annealing, the TiO_2 nanotubes were amorphous, which only demonstrates the diffraction peaks from ITO glass (JCPDS Card no. 39-1058). After annealing at 400 °C for 1 h in air, the TiO_2 nanotubes had anatase phase (JCPDS Card no. 84-1286) and there is no diffraction peaks indicating that ZnO templates completely removed by the final step of wet etching. On the basis of the XRD data, the final TiO_2 nanotubes were found to consist of ~19.4 nm (Scherrer equation[33]) anatase nanocrystals.

Apart from the XRD patterns, energy dispersive X-ray (EDX) before and after the formation of TiO_2 nanotubes was further used to reveal the formation of TiO_2 and elimination of the ZnO template. Figure 2 shows the EDX spectra, where Zn and Ti contents were analyzed on the ZnO nanorods and TiO_2 nanotubes, respectively. The absence of a peak at ~1 keV, corresponding to Zn, of the EDX spectra taken from TiO_2 nanotubes indicates the removal of the ZnO nanorod template.

Figure 3a,b shows the top view SEM images of the ZnO nanorod and TiO_2 nanotube film. As shown in Figure 3a, highly uniform and well-spaced arrays of ZnO nanorods were successfully formed with preferential growth in the *c*-axis orientation (0001). Each nanotube is about 20−30 nm in diameter and ~150−200 nm in length. The structure of ZnO nanorods was found to be very sensitive to the processing parameters, including the precursor concentration, growth temperature, and time. The SEM images of ZnO nanorods prepared by varying the concentration and growth time show in Figure 4. This

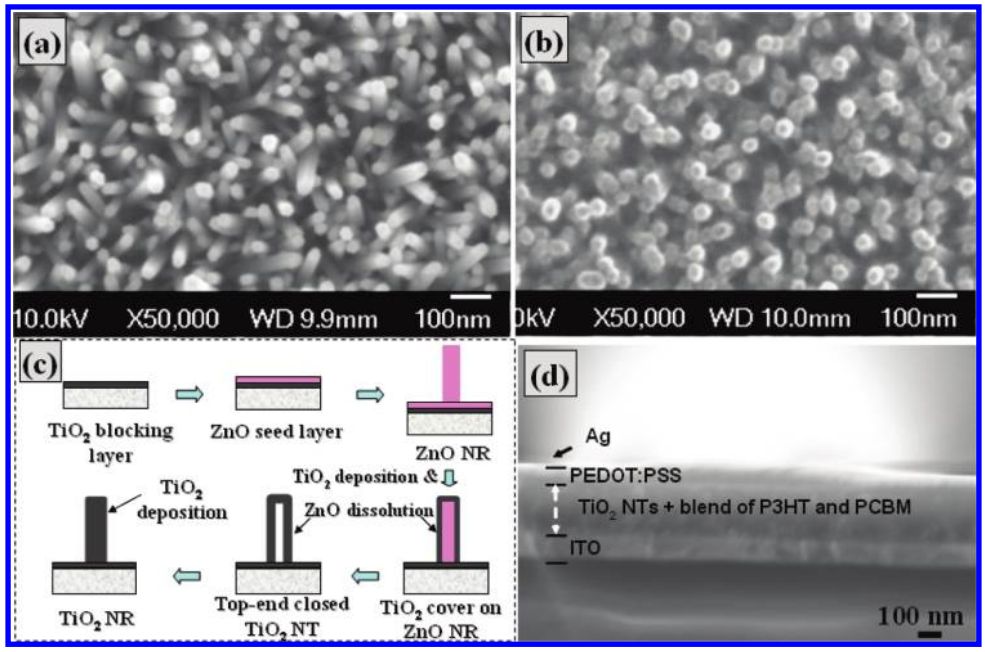

Figure 3. (a,b) The top view SEM images of ZnO nanorods and TiO_2 nanotubes, respectively, (c) the schematic process of preparing TiO_2 nanotubes, and (d) the cross section of hybrid solar cell photoelectrode using TiO_2 nanotubes.

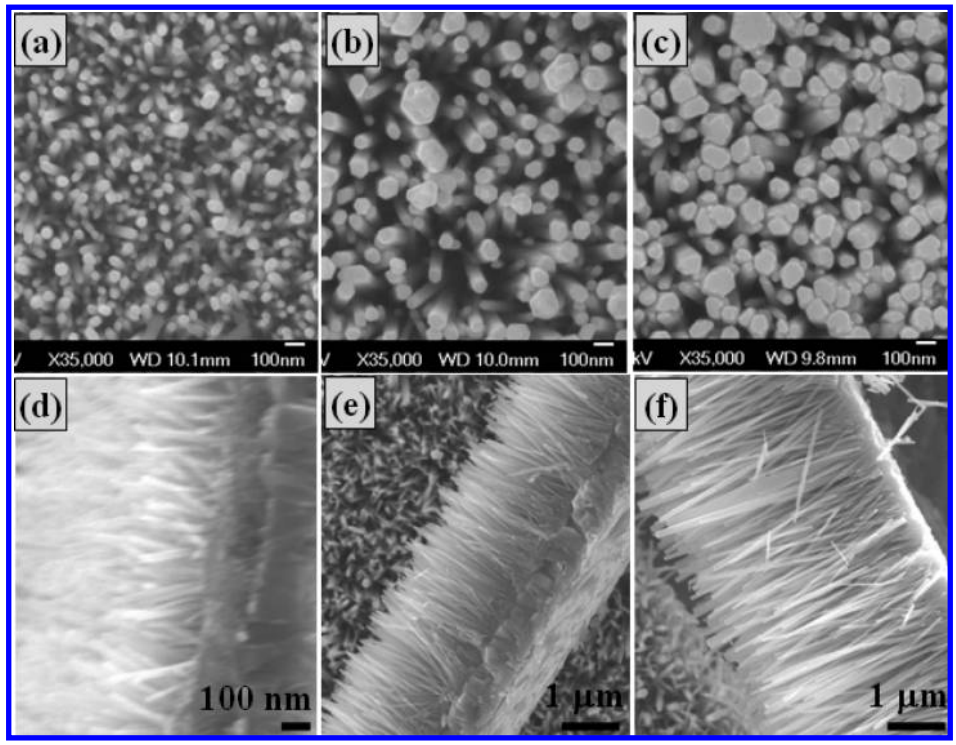

Figure 4. (a−c) The top view SEM images of ZnO nanorods prepared by varying the concentration of $Zn(NO_3)_2$ at 0.025, 0.050, and 0.100 M, respectively; (d−f) the cross section SEM images of ZnO nanorods prepared by using 0.015 M $Zn(NO_3)_2$ and varying growth time at 2, 6, and 12 h, respectively.

observation is consistent with the results reported in literature.[34] It was found that the length of ZnO nanorods can be controlled by varying the growth time in ZnO precursor solution. Particularly, the length of ZnO nanorods increases when extending the growth time, as shown in Figure 4d−f. Meanwhile, the diameter of nanorod is independent of the reaction time and mainly tailed by the concentration of zinc source. These ZnO nanorods were subsequently converted to TiO_2 nanotubes via the liquid-phase deposition in an aqueous solution consisting of $(NH_4)_2TiF_6$ and H_3BO_3. It is reasonable to assume that, under optimized conditions, the ZnO layer could be completely removed and the TiO_2 nanotubes retain the length and diameter of the ZnO template. The formation of TiO_2 is believed to proceed via the following equation eq 1[35,36]

$$TiF_6^{2-} + 2H_2O \leftrightarrow TiO_2 + 6F^- + 4H^+ \qquad (1)$$

This reaction can be shifted to the right by adding H_3BO_3, which reacts with F^- ions and form a more stable complex ions, BF_4^-, as outlined in eq 2

$$H_3BO_3 + 4H^+ + 4F^- \leftrightarrow BF_4^- + H_3O^+ + 2H_2O \quad (2)$$

ZnO nanorods will dissolve into the solution by react with H_3O^+ and this process resulted in the formation of a TiO_2 nanotubes with the top-end closed

$$ZnO + 2H_3O^+ \rightarrow Zn^{2+} + 3H_2O \quad (3)$$

The deposition TiO_2 on the ZnO nanorod template and the removal of ZnO nanorods proceed simultaneously.[35] The deposition of TiO_2 continued to fill the void space within the TiO_2 tubule and the TiO_2 nanorod could finally be obtained, when the deposition time is sufficiently long. The resultant TiO_2 nanotubes were further immersed in a H_3BO_3 solution to ensure the complete removal of any residual ZnO. The pH of the solution is very sensitive to the dissolution of ZnO nanorods. The decrease in pH value of the solution accelerates the dissolution of ZnO nanorods and will result in a lower array density of TiO_2 nanotubes.[36]

As indicated in Figure 3b, it is observed that the diameter of TiO_2 nanotubes is in the range of ~20−35 nm, which provides a large specific surface area. It should be noted that although the SEM topography shows the nanotube morphology, it is possible that the lower part (close to substrate) of the TiO_2 nanotubes is filled up to form nanorods. The length of TiO_2 nanotubes was controlled to be typically 150−200 nm for an optimal hybrid photovoltaic device performance as there is a trade-off between the distance that charge carriers need to travel to reach respective collection layer and the maximized light absorption.[20] In addition, it is noticed that the TiO_2 nanotube film possessed a very porous structure, that is, the nanotubes are well separated from one another, which allows the efficient infiltration of polymer solution. Figure 3c shows the schematic process involving the growth of barrier TiO_2 layer, the ZnO seed layer, ZnO nanorods, and the deposition of TiO_2 nanotubes and simultaneous ZnO dissolution.

Since the work function of ITO (4.5−4.7 eV) is intermediate between the work function of HOMO and LUMO of P3HT, ITO can collect either electrons or holes. The compact TiO_2 layer at the bottom of the nanotubes will function as a hole-blocking layer to prevent the holes from reaching to the transparent conductive ITO substrates.[37] Figure 3d shows the cross-section image of TiO_2 nanotubes hybrid solar cell: Ag/PEDOT−PSS/blend of P3HT−PCBM/TiO_2 NTs/ITO.

Figure 5 shows the current density−voltage curves of the hybrid solar cells based on the TiO_2 nanotubes infiltrated with a blend of P3HT and PCBM. For a better comparative study, the hybrid solar cell using ZnO nanorods was prepared under identical processes. The values of short-circuit current density (J_{sc}), open-circuit voltage (V_{oc}), fill factor (FF), and overall power conversion efficiency (η) are summarized in Table 1. One approach to improve the performance of hybrid solar cell is to manipulate the dimensions of TiO_2 nanotubes, which is determined by the ZnO nanorod template. It was found that the typical maximum efficiency was obtained when growing TiO_2 nanotubes with about 25−35 nm in diameter and ~150−200 nm in length. With too short and/or too small TiO_2 nanotubes, the cells showed much lower performance and vice versa. As demonstrated in Figure 5, the highest performed hybrid solar cells was achieved with V_{oc} = 646 mV, J_{sc} = 9.96 mA cm^{-2}, FF = 51.6%, PCE = 3.32% for the TiO_2 nanotubes annealed at 400 °C in conjunction with P3HT/PCBM. The PCE of 3.32%

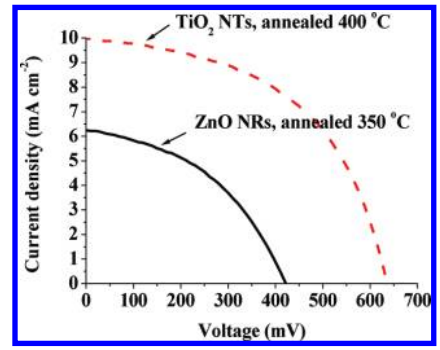

Figure 5. The current density−voltage curves of the hybrid solar cells of the ZnO nanorods and TiO_2 nanotubes infiltrated with a blend of P3HT and PCBM.

TABLE 1: Performances of the Solar Cells with the Electrode Made of ZnO Nanorods and TiO_2 Nanotubes

samples	V_{oc} (mV)	J_{sc} (mA cm^{-2})	FF (%)	η (%)
ZnO nanorods, annealed 350 °C for 1 h	432	6.28	43.76	1.19
TiO_2 nanotubes, annealed 400 °C for 1 h	646	9.95	51.60	3.32

achieved in this work is significantly higher than 0.7% of the same type structured hybrid solar cells reported in literature.[31]

Charge separation in our hybrid solar cell occurs both at the interface between P3HT and PCBM and the interface between P3HT and TiO_2, a double heterojunction structure as shown in Figure 6. TiO_2 nanotubes help to reduce the electron recombination and function as the direct pathway for fast electron transport to the charge collecting electrode, promising better power conversion efficiency.

The barrier layer of TiO_2 at the bottom keeps the holes from touching the ITO substrates so as to increase the charge collection. As a result, the short circuit current density and open circuit voltage were remarkably enhanced. On the other hand, the hybrid solar cells based on ZnO nanorod/P3HT/PCBM exhibited V_{oc} of 432 mV, J_{sc} of 6.28 mA cm^{-2}, FF of 43.76%, PCE of 1.19%, respectively, which are comparable to 1.16% reported by Rattanavoravipa et al.[38] Obviously, the V_{oc}, $J_{sc,}$ and FF of the dye-sensitized solar cell using ZnO nanorods are significantly lower than that of TiO_2 nanotubes.

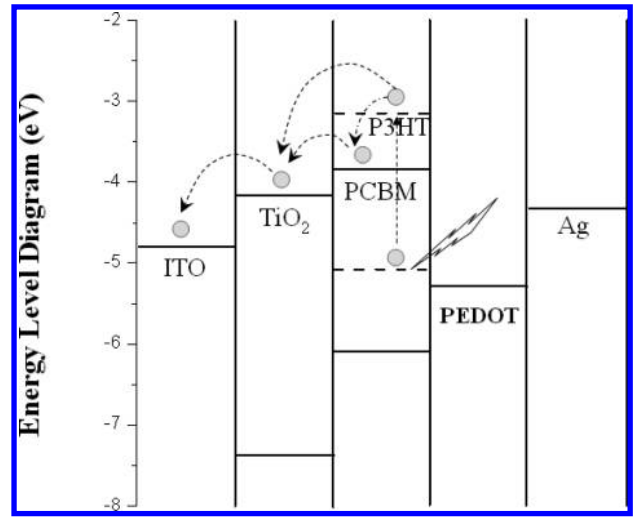

Figure 6. Schematic representation energy diagram of double heterojunction photovotaic device, ITO/TiO_2/blend P3HT−PCBM/PEDOT/Ag.

It should be noted that the enhanced power conversion efficiency in this hybrid solar cells could be attributed to (1) the suitable oriented TiO_2 nanotubes for the hybrid solar cell, exciton diffusion length, and (2) the oriented TiO_2 nanotubes reduced the electron recombination by provided a direct pathway for fast electron transport to the charge collecting electrode. In addition, the further improved the PCE could be with the consideration of the following factors: (1) ideal TiO_2 nanotubes grown perpendicular to the ITO substrates via manipulating the densities of TiO_2 nanotube, and (2) interface modification and better infiltration of polymer into TiO_2 nanotubes[39] to improve charge separation and reduce electron recombination by tuning the polymer blend concentration, the ratio of P3HT to PCBM, spin-coat process, and polymer annealing treatment.[40]

Conclusions

High-power conversion efficiency in solid-state inorganic−organic solar cells that dense TiO_2 nanotubes filled with a blend of P3HT/PCBM as the active layer has been demonstrated. The presence of P3HT−TiO_2 heterojunction provides an additional interface as compared to conventional polymer-based photovoltaics. The resulting solar cells showed a short-circuit current density of 9.95 mA cm^{-2}, open circuit voltage of 646 mV, and a fill factor of 51.6%, leading to a power conversion efficiency of 3.32%, much higher than 0.7% reported in literature. Such an enhancement in power conversion efficiency is attributed to smaller diameter of TiO_2 nanotubes with a high density, yet well spaced for efficient penetration of polymer solution. Further improvement in device performance can be achieved by growing vertically oriented TiO_2 nanotube array and/or by organic/inorganic interface modification.

Acknowledgment. This work has been supported by the Institute for the Promotion of Teaching Science and Technology (IPST), the Center of Excellence for Innovation in Chemistry (PERCH-CIC), the Commission on Higher Education, Ministry of Education, a Mahidol University Research Grant, the Thailand Center of Excellence in Physics (ThEP), the U.S. Department of Energy, Division of Materials and Engineering under Award No. DE-FG02-07ER46467 (Q.F.Z.), National Science Foundation (DMR 1035196), the University of Washington TGIF grant, the Washington Research Foundation, and the Intel Corporation.

References and Notes

(1) Huynh, W. U.; Dittmer, J. J.; Alivisatos, A. P. *Science* **2002**, *295*, 2425.
(2) Zhang, Q. F.; Dandeneau, C. S.; Zhou, X. Y.; Cao, G. Z. *Adv. Mater.* **2009**, *21*, 4087.
(3) Yodyingyong, S.; Zhang, Q. F.; Park, K.; Dandeneau, C. S.; Zhou, X. Y.; Triampo, D.; Cao, G. Z. *Appl. Phys. Lett.* **2010**, *96*, 073115.
(4) Helgesen, M.; Sondergaard, R.; Krebs, F. C. *J. Mater. Chem.* **2010**, *20*, 36.
(5) Günes, S.; Neugebauer, H.; Sariciftci, N. S. *Chem. Rev.* **2007**, *107*, 1324.
(6) Cheng, Y. J.; Yang, S. H.; Hsu, C. S. *Chem. Rev.* **2009**, *109*, 5868.
(7) Snaith, H. J.; Moule, A. J.; Klein, C.; Meerholz, K.; Friend, R. H.; Grätzel, M. *Nano Lett.* **2007**, *7*, 3372.
(8) Po, R.; Maggini, M.; Camaioni, N. *J. Phys. Chem. C* **2009**, *114*, 695.
(9) Lewis, N. S. *Science* **2007**, *315*, 798.
(10) Cai, W.; Gong, X.; Cao, Y. *Sol. Energy Mater. Sol. Cells* **2010**, *94*, 114.
(11) Solarmer Energy, Inc. http://www.solarmer.com/ (accessed September 14, 2010).
(12) Shao, S.; Liu, F.; Xie, Z.; Wang, L. *J. Phys. Chem. C* **2010**, *114*, 9161.
(13) Scully, S. R.; McGehee, M. D. *J. Appl. Phys.* **2006**, *100*, 034907.
(14) Yang, F.; Shtein, M.; Forrest, S. R. *Nat. Mater.* **2005**, *4*, 37.
(15) Wienk, M. M.; Turbiez, M. G. R.; Struijk, M. P.; Fonrodona, M.; Janssen, R. A. J. *Appl. Phys. Lett.* **2006**, *88*, 153511.
(16) Markus, K.; Hans-Joachim, E.; Gilles, D.; Markus, C. S.; Christoph, J. B.; Pavel, S.; Claudia, N. H. *Adv. Funct. Mater* **2010**, *20*, 338.
(17) Yongye, L.; Zheng, X.; Jiangbin, X.; Szu-Ting, T.; Yue, W.; Gang, L.; Claire, R.; Luping, Y. *Adv. Mater.* **2010**, *22*, 1.
(18) Mor, G. K.; Kim, S.; Paulose, M.; Varghese, O. K.; Shankar, K.; Basham, J.; Grimes, C. A. *Nano Lett.* **2009**, *9*, 4250.
(19) Briseno, A. L.; Holcombe, T. W.; Boukai, A. I.; Garnett, E. C.; Shelton, S. W.; Frechet, J. J. M.; Yang, P. *Nano Lett.* **2009**, *10*, 334.
(20) Greene, L. E.; Law, M.; Yuhas, B. D.; Yang, P. *J. Phys. Chem. C* **2007**, *111*, 18451.
(21) Ravirajan, P.; Peiro, A. M.; Nazeeruddin, M. K.; Grätzel, M.; Bradley, D. D. C.; Durrant, J. R.; Nelson, J. *J. Phys. Chem. B* **2006**, *110*, 7635.
(22) Zhu, R.; Jiang, C. Y.; Liu, B.; Ramakrishna, S. *Adv. Mater.* **2009**, *21*, 994.
(23) Shankar, K.; Mor, G. K.; Prakasam, H. E.; Varghese, O. K.; Grimes, C. A. *Langmuir* **2007**, *23*, 12445.
(24) Yu, B. Y.; Tsai, A.; Tsai, S. P.; Wong, K. T.; Yang, Y.; Chu, C. C.; Shyue, J. J. *Nanotechnology* **2008**, *19*, 255202.
(25) Chen, C.; Wang, M.; Wang, K. *J. Phys. Chem. C* **2009**, *113*, 1624.
(26) Otsuka, Y.; Okamoto, Y.; Akiyama, H. Y.; Umekita, K.; Tachibana, Y.; Kuwabata, S. *J. Phys. Chem. C* **2008**, *112*, 4767.
(27) Shankar, K.; Mor, G. K.; Prakasam, H. E.; Varghese, O. K.; Grimes, C. A. *Langmuir* **2008**, *24*, 14321.
(28) Mor, G. K.; Shankar, K.; Paulose, M.; Varghese, O. K.; Grimes, C. A. *Appl. Phys. Lett.* **2007**, *91*, 152111.
(29) Shankar, K.; Mor, G. K.; Paulose, M.; Varghese, O. K.; Grimes, C. A. *J. Non-Cryst. Sol.* **2008**, *354*, 2767.
(30) Yang, D. J.; Kim, H. G.; Cho, S. J.; Choi, W. Y. *Mater. Lett.* **2008**, *62*, 775.
(31) Rattanavoravipa, T.; Sagawa, T.; Yoshikawa, S. *Sol. Energy Mater. Sol. Cells* **2008**, *92*, 1445.
(32) Park, J. H.; Kim, J. S.; Lee, J. H.; Lee, W. H.; Cho, K. *J. Phys. Chem. C* **2009**, *113*, 17579.
(33) Fujihara, K.; Kumar, A.; Jose, R.; Ramakrishna, S. *Nanotechnology* **2007**, *18*, 365709.
(34) Qiu, J. J.; Yu, W. D.; Gao, X. D.; Li, X. M. *Nanotechnology* **2006**, *17*, 4695.
(35) Xu, C.; Shin, P. H.; Cao, L.; Wu, J.; Gao, D. *Chem. Mater.* **2009**, *22*, 143.
(36) Lee, J. H.; Leu, I. C.; Hsu, M. C.; Chung, Y. W.; Hon, M. H. *J. Phys. Chem. B* **2005**, *109*, 13056.
(37) Boucle, J.; Ravirajan, P.; Nelson, J. *J. Mater. Chem.* **2007**, *17*, 3141.
(38) Rattanavoravipa, T.; Chareonsirithavorn, P.; Sagawa, T.; Yoshikawa, S. *Solid-State Electron.* **2009**, *53*, 176.
(39) Tepavcevic, S.; Darling, S. B.; Dimitrijevic, N. M.; Rajh, T.; Sibener, S. J. *Small* **2009**, *5*, 1776.
(40) Ballantyne, A. M.; Ferenczi, T. A. M.; Campoy-Quiles, M.; Clarke, T. M.; Maurano, A.; Wong, K. H.; Zhang, W.; Stingelin-Stutzmann, N.; Kim, J. S.; Bradley, D. D. C.; Durrant, J. R.; McCulloch, I.; Heeney, M.; Nelson, J.; Tierney, S.; Duffy, W.; Mueller, C.; Smith, P. *Macromolecules* **2010**, *43*, 1169.

JP1077888